AIAA-91-1118-CP

STRAIN RATE SENSING FOR VIBRATION CONTROL OF FLEXIBLE STRUCTURES

John M. Juston*
David P. Bauer
IAP Research, Inc.
2763 Culver Avenue
Dayton, OH 45429-3723

Abstract

Low mass, high performance strain rate sensing technology is presented. This is an enabling sensor technology for the active control of vibrating structures. The sensor is based on electromagnetic technology and has an output directly proportional to strain rate. It either attaches to or imbeds in a structure. Here, sensor physics are discussed and its sensitivity equation is derived. We present strain rate sensing performance requirements which we have distilled from ongoing structural control experiment needs. Proof-of-principle experiments integrate the sensor with a beam structure to measure beam structural strain rates during oscillatory loading. The experiments demonstrate favorable strain rate resolution while measuring 80 μstrain, 0.1 Hz structural oscillations. Superior resolution is demonstrated while measuring larger strain rate magnitudes occurring during 16 μstrain, 20 Hz oscillations. Sizing estimates indicate that sensor mass can be made very small; easily less than 20 grams for the applications we've studied. Key technical challenges from our ongoing development effort are also discussed.

Introduction

Proposed future space structures[1,2] establish active control of structural vibrations as an essential technology. In recent years, the structural vibration control mission has motivated significant efforts in control theory research[3]. In addition to control theory advances, sensor and actuator technologies must also be furthered to meet high precision, low mass mission requirements. The research presented in this paper focuses on the development of an enabling sensor technology for implementing active control on vibrating structures.

Many control theory endeavors assume availability of displacement and velocity sensors for implementation of a full state feedback control law[4-6]. In practice, measurement of position states has traditionally not posed a problem. A common approach is to use strain gages for determining position state magnitudes during vibration. Local strain data can be related directly to eigenvector magnitudes in the state model. This has been successfully applied in numerous experimental investigations.[7-9] Although there has been some reported difficulties with noise and 60 Hz sensitivity,[10] for the most part the results are good.

Sensing velocity data has not been as successful. In fact, it is generally acknowledged in the control of structures community[11] that there is a lack of adequate rate sensing technology. Common approaches for arriving at vibratory rates include differentiating displacement data (such as from strain gage) or implementing state estimators. The noise inherent in these signals renders velocity data useless. This has been attempted, with unsatisfactory results many times over the years.[7,12-14]

Non-contacting rate sensors have been used successfully in collocated control loops.[15] The non-contacting rate sensors required an attachment external to the vibrating structure itself. In general, this is undesirable; it is also not practical for space applications. However, the guaranteed system stability of collocated rate feedback[16,17] appeals for structurally integral, high resolution, vibratory rate sensing capability.

The goal of our research effort is to develop low mass, high performance strain rate sensor technology to measure structural vibration rates. Strain rate sensors are currently not commercially available simply because there has been no prior demand. In essence, real-time strain rate sensing is a problem unique to active structural vibrations control requirements.

In this paper, we discuss the strain rate sensor technology under development at IAP Research. Our strain rate sensing concept is based on electromagnetic technology. It is called the Variable Reluctance Transformer (VRT) Strain Rate Sensor. Our sensor attaches to or imbeds in a structure, depending on the application. Its output is a clean, direct measurement of structural strain rate. We have already demonstrated concept feasibility. We are currently developing a low mass, high performance strain rate sensor prototype that satisfies structural vibration control performance requirements.

This paper is divided into five sections. In the first section, we describe VRT Strain Rate Sensor

---

* Member AIAA

fundamentals and derive its sensitivity equation. We briefly review its historical roots and compare it to other electromagnetic-based sensors. Next, we review our strain rate sensing performance objectives that we have distilled from ongoing structural control experiments and spacecraft design needs. We review our proof-of-principle test results and analyze sensor mass estimates. The tests demonstrate relevant bandwidth and resolution capabilities with our sensor concept. The sizing estimates indicate that sensor mass can be made small: easily less than 20 grams for the applications we've studied. Finally, we briefly review unresolved technical issues which govern our ongoing research.

VRT Strain Rate Sensor

Concept Description

VRT Strain Rate Sensor technology is based on Faraday's Law. A changing magnetic field in a wire loop induces a voltage (emf) in the loop. The induced voltage is proportional to the time rate of change of magnetic flux in the loop.

A schematic drawing of the sensor concept is shown in Figure 1. It consists of an excitation and output winding on two ferromagnetic cores. The ferromagnetic cores are separated by a small air gap. The two ferrocores and air gaps form a magnetic circuit. The magnetic circuit reluctance (resistance to magnetic flow) is determined primarily by the air gaps. The excitation coil provides a constant magnetomotive force (mmf) that establishes a DC magnetic field in the magnetic circuit. The magnetomotive force can also be provided by a permanent magnet. The ferrocores attach to a structures' surface such that surface strain varies the length of the air gap. Since the mmf is constant, the magnetic field through the output winding varies with strain. Hence, the voltage across the winding varies with strain rate.

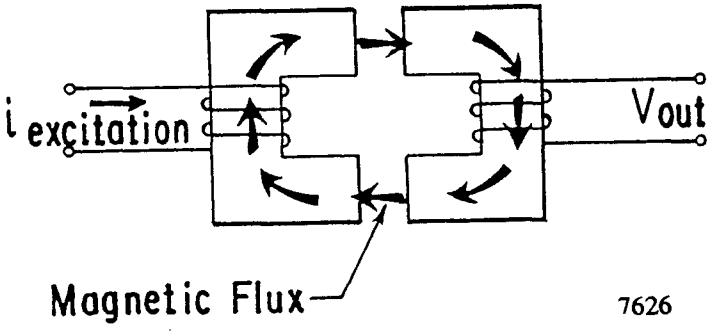

Fig. 1. In the VRT Strain Rate Sensor, magnetic field magnitude is highly sensitive to air gap length.

The sensor attaches at the outside edges of the ferrocores. Therefore, the gage length is typically several orders of magnitude greater than the gap length. The "apparent" strain in the air gap becomes the surface strain amplified by the ratio of gage to gap lengths. This is the key to low mass designs.

The sensor geometry is very flexible. It need not have the "square" appearance of the cores in the schematic diagram. The two important geometric ingredients in implementing this concept are the small air gap and larger gage length. VRT strain rate sensors incorporated in smart strut applications will work with the same physics but have very different configurations.

Our research on this sensor has so far been a proof-of-principle effort. The remainder of this paper discusses results based on the relatively simple geometry of Figure 1.

Sensitivity Derivation

Faraday's law is most simply expressed as

$$V_{out} = N \frac{d\Phi}{dt} \qquad (1)$$

where V_{out} = induced voltage,
N = number of wire turns in output winding,
Φ = magnetic flux in circuit, and
t = time.

Using the chain rule, we can expand the time derivative of flux to

$$\frac{d\Phi}{dt} = \frac{d\Phi}{d\epsilon}\frac{d\epsilon}{dt} \qquad (2)$$

where ϵ = strain.

Substituting into Equation 1 gives a fundamental expression for sensor sensitivity

$$\frac{V_{out}}{\dot{\epsilon}} = N \frac{d\Phi}{d\epsilon} \qquad (3)$$

where $\dot{\epsilon}$ = strain rate.

We now examine flux to express it in terms of physical parameters. Magnetic flux is defined as

$$\Phi = \frac{mmf}{\mathbf{R}} \qquad (4)$$

where mmf = magnetomotive force, and
$\mathbf{R}$ = magnetic circuit reluctance.

Reluctance is the magnetic circuit analog of resistance. For the magnetic circuit in Figure 1, circuit reluctance is the sum of the core and gap reluctances. Expressing reluctance in terms of geometric variables gives

$$\mathbf{R} = \frac{\ell_g}{\mu_0 A} + \frac{\ell_c}{\mu_c A} \qquad (5)$$

where ℓ_g = total gap length,
μ_0 = magnetic permeability of air (gap),
ℓ_c = total core length,
μ_c = magnetic permeability of core, and
A = core and gap cross sectional area.

The ferromagnetic cores attach to the structure making gap length, ℓ_g, strain sensitive. Since all strain occurring within the gage length appears as a change in gap length, the time variant gap length is written as

$$\ell_g = \ell_0 + \epsilon L_g \qquad (6)$$

where ℓ_0 = nominal air gap length, and
L_g = gage length.

Since the gage length is significantly larger than the gap length, magnetic flux experiences appreciable fluctuations from its nominal magnitude. We represent the field as a sum of its nominal value and a strain related perturbation. Substituting Equations 5 and 6 into Equation 4, a Taylor series expansion about the nominal gap length, ℓ_o, reduces to

$$\Phi = \Phi_0[1 - (\epsilon K) + (\epsilon K)^2 - (\epsilon K)^3 + \ldots] \qquad (7)$$

where we define

$$\Phi_0 = \frac{mmf}{\mathbf{R}_o} \qquad (8)$$

and,

$$K = \frac{L_g/\ell_0}{1 + \frac{\ell_c \mu_0}{\ell_0 \mu_c}} \qquad (9)$$

The second term in the denominator of the constant K is simply the ratio of the magnetic reluctances of the gap and core. In most applications, the core reluctance is insignificant compared with the air gap reluctance. In these cases, the denominator of K is approximately 1. With this assumption in mind, K takes on more meaning as simply the ratio of gage to gap lengths; in other words, K approximates the strain amplification in the gap.

$$K \approx \frac{L_g}{\ell_o} \qquad (10)$$

Returning to our derivation, Equation 7 is recognized as a binomial expansion which compresses to

$$\Phi = \frac{\Phi_0}{1 + \epsilon K} \qquad (11)$$

We can now more easily evaluate Equation 3 and arrive at the sensitivity expression,

$$\frac{V}{\dot{\epsilon}} = \frac{-KN\Phi_0}{(1 + \epsilon K)^2} \qquad (12)$$

Magnetic flux, Φ_0, is still a relatively intangible design variable. Flux can be expressed as the product of flux density, β, and core cross-sectional area, A,

$$\Phi_0 = \beta_0 A \qquad (13)$$

where β_0 = nominal magnetic flux density.

Ferro-magnetic materials are relatively linear when their flux density is below about 2 Tesla (20,000 gauss). We want to operate in this regime. With flux density limited, flux is chiefly determined by core area. Making a final substitution yields a more tangible sensitivity equation,

$$\frac{V}{\dot{\epsilon}} = \frac{-KNA\beta_0}{(1 + \epsilon K)^2} \qquad (14)$$

where β_0 = nominal magnetic field density.

There are two important characteristics of the derived sensitivity to note at this time. First, sensitivity is directly proportional to size variables. As core area, number of turns, and gage-to-gap length ratio increase so does sensitivity. These variables can all be correlated to an increase in sensor mass.

Secondly, sensitivity is inherently nonlinearly dependent on time-variant strain. Structural strain oscillations are ninety degrees out of phase with strain rates. This will tend to distort the output waveform of our strain rate sensor. This is undesirable. The

magnitude of the nonlinearity is dictated by the gage to gap length ratio. If this ratio is made unity, the nonlinearity would have little impact on output waveform. However, unity gage-to-gap ratio would decrease sensitivity and adversely affect sensor mass.

Strain amplitudes also dictate waveform distortion. Stiff structures typically have small strain amplitudes oscillating at high frequencies. Output waveform is not nearly as affected in this case as for "softer" structures where strain amplitudes are relatively high. Post-processing sensor output is an undesirable option in dealing with this inherent nonlinearity. Our ongoing research efforts are examining alternative geometries that potentially minimize nonlinear magnitudes. For the remainder of this paper, we assume the ϵK product is small enough to neglect. This assumption may not always be correct, but it does not effect the results of our proof-of-principle feasibility investigation.

Historical Perspective

Position and velocity sensors have been designed based on electromagnetic principles since around the turn of the century[18]. One sensor, the magnetic strain gage,[19,20] is a variable reluctance EM sensor that was introduced around 1930. The geometry and operational principles are very similar to our VRT Strain Rate Sensor. The key difference is that this device is sensitive to micro-displacements (strain) and not to micro-velocities (strain rate).

Instead of a constant mmf, a sinusoidal input voltage establishes a sinusoidal magnetic flux in this sensor. The amplitude of the coupled output oscillations depends on the air gap length. As with our sensor, this sensor attaches directly to the structure. The output signal is demodulated for strain measurement. The magnetic strain gage was a dominate strain gaging technique throughout the 1930's and 1940's. It was widely used for experimental stress analysis on ship and railroad designs. In the 1940's, bonded foil resistance strain gage techniques emerged. By virtue of its application ease and very small, unobtrusive size, the bonded strain gage became very popular. Eventually, the bonded foil resistance gage became so widely accepted that it dominated the strain gage field. Obviously, this is still true today. The magnetic strain gage has only rarely been used since then. Hetenyi[21] states that the variable air-gap geometry is one of the best-known methods of converting small motions into high electric signals.

Today, there are several commercially available sensors that use variable reluctance technology for measuring velocity. Seismic velocity transducers (used for detecting vibrations in heavy machines) and Linear Velocity Transducers (LVT's) are good examples. The geometry of these sensors is similar to one another but quite different from our strain rate sensor. Typically, they vary the position of a permanent magnet within a concentric output coil. Voltage is induced in the coil proportional to the rate at which the magnet moves. This geometry has good linearity and is a good means for measuring velocity. However, relatively large air paths in the magnetic circuit limit sensitivity to very small velocities. A small air gap configuration, such as our strain rate sensor, is about 100 times more sensitive to very small motions than a concentric core configuration[22,23]. It is interesting to note that our sensor would be a poor design for measuring velocities that occur over greater distances. As we have seen, our output becomes highly nonlinear with larger "bulk" motions.

Finally, it should also be mentioned that EM velocity sensors have been used before in vibration control experiments[15]. These were relatively large voice coil-like devices that detected local velocity of the vibrating structure. As mentioned before, this application required external mounting from the vibrating structure itself and hence was not well suited to real applications.

Strain Rate Sensor Performance Objectives

Design Philosophy

IAP Research is developing low mass, high performance Strain Rate Sensor technology to measure structural vibration rates. An ideal sensor design would have infinite bandwidth, unlimited resolution, infinite signal-to-noise ratio, and zero mass. Realistically, a sensor design is confronted with tradeoffs that inevitably compromise ideal performance. Therefore, we strive to set realistic performance goals that will bound our design tradeoffs. Our design philosophy is to minimize sensor mass while meeting realistic performance specifications.

Desirable performance specifications were distilled from conversations with test engineers and sensor manufacturers. We define two sets of performance objectives: mission dependent objectives and precision and accuracy objectives. Mission dependent objectives are specific to structural control applications. These parameters include resolution and bandwidth, and limitations on acceptable sensor mass. Precision and accuracy objectives include good linearity, low cross-sensitivity, and desirable signal-to-noise ratio. This section defines objectives for high performance strain rate sensing on vibrating structures.

Mission Defined Objectives

Resolution, bandwidth and sensor intrusiveness (in this case measured by mass) are the three parameters that primarily dictate sensor choice for a given application. Most sensor manufacturers do not have the luxury of a beforehand knowledge of specific applications during design. Therefore, general "families" of sensors are designed. In turn, test engineers choose a "best fit" from these families for their application. We have been

communicating directly with test engineers to ensure relevance of our VRT Strain Rate Sensor design for active vibration control applications. Structural control engineers will benefit directly from a sensor design tailored to their needs.

We are soliciting data from a total of five experimental applications. In this paper we describe strain rate sensing performance guidelines for two of these applications.

JPL's structural control mission[24] focuses on developing lightweight structures with superior stability and precision. Dr. James Fanson of JPL has provided "back-of-the-envelop" estimates of resolution, bandwidth, and mass requirements for precision truss applications[25]. He estimates that minimum strain rate resolution requirements might entail measurement of 1 μstrain (tensile/compressive) occurring at 4 Hz first mode oscillation frequencies. This gives a strain rate resolution requirement of about 25 e^{-6} ϵ/s. At least 40 dB (preferably 60 dB) signal-to-noise ratio is necessary at this resolution. Since actuator dynamics extends into the kilohertz range, sensor bandwidth should incorporate at least the same range. Finally, a sensor mass of less than 20 grams will be "non-costly" in current precision truss applications.

Dr. Harry Robertshaw at Virginia Tech has provided similar data for his plate acoustic vibration control experiments[26]. Strain rates are induced in this experiment by bending mode oscillations. He assessed a resolution requirement of about 60 e^{-6} ϵ/s based on 0.2 μstrain at plate center during first mode 50 Hz oscillations. The highest modelled structural mode is around 345 Hz. He suggested a 350 Hz strain rate sensor bandwidth provided there is no appreciable gain or phase error. Currently, 4 gram accelerometers on the experiment are included in his structural dynamics models. He emphasized that in simple geometric applications, modelling sensor mass along with the rest of the structure is not a problem.

A summary of these guidelines for mission defined strain rate sensing goals is in Table 1.

Accuracy and Precision Objectives

Accuracy and precision objectives serve a different function than mission defined objectives; they assure quality in VRT Strain Rate Sensor output. The three key accuracy and precision parameters are linearity, cross-sensitivity, and signal-to-noise ratio.

TABLE 1

DESIGN GUIDELINES FOR STRAIN RATE SENSING APPLICATIONS

Facility	Application	Resolution (Strain/s)	Bandwidth (Hz)	Mass (g)
JPL	precision truss	25E-06	4-1000's	<20
VA Tech Dr.Robertshaw	vibrating plate	60E-06	50-345	can include in FE model

Realistic linearity and cross-sensitivity values were obtained by surveying specifications for commercially available sensors. We reviewed about 50 commercially available LVDT's, LVT's, strain gages, accelerometers, vibration transducers, and rate gyros. We found strain gages demonstrate superior linearity and cross-sensitivity. Mechanical hysteresis in the gage is the main source of output nonlinearities. Depending on adhesives, hysteresis is typically less than 1 μstrain. For most applications, this hysteresis can be zeroed out after the sensor is broken in. For all practical purposes, strain gages are nearly perfectly linear. Their cross-sensitivity is also very low at less than 0.1%. LVDT's are also precision devices. Their linearity is typically within 0.2-1%. LVDT cross-sensitivity is also in the 0.2% range. On the other extreme are commercial vibration transducers. These devices are not used in precision applications. Output deviates up to 5% from linear and cross-sensitivity is as high as 10%. We feel realistic design goals for linearity deviations and cross-sensitivity is to keep both values below 1%.

Signal-to-noise (S/N) criteria insures fine signal quality for each strain rate sensor application. Most sensors have essentially infinite resolution; some input to the sensor will produce some output voltage (no matter how small). This is also true for our strain rate sensor. In practice then, measurement resolution is limited by noise characteristics. Noise introduced at any point in the signal path is detrimental. Electromagnetic pickup, thermal noise, amplifier and signal conditioning noise all limit sensor resolution capabilities. A sensor resolution specification is meaningless without a corresponding signal-to-noise specification. Our feeling is that minimum acceptable signal quality requires a 40 dB S/N ratio with a clear understanding that more is better.

A summary of our performance goals for linearity, cross-sensitivity, and signal-to-noise ratio are given in Table 2.

TABLE 2

DESIGN GUIDELINES FOR

ACCURACY & PRECISION

PARAMETERS	OBJECTIVE
linearity error	<1%
cross-sensitivity	<1%
S/N	>40 dB

Proof-of-Principle Testing and Sizing Estimates

We performed tests with a proof-of-principle sensor design to demonstrate resolution and bandwidth capabilities. We also estimated sensor mass as a function of resolution using a simple transformer mass optimization technique. Taken together, these results demonstrate the feasibility of our strain rate sensor for rate sensing on flexible structures.

Test Setup

We performed strain rate sensing experiments at the Structural Test Laboratory (STL) which is a subdivision of the Experimental and Applied Mechanics Division of the University of Dayton Research Institute. The load frames maintained at STL have the capability for applying precisely controlled linear or rotary forces, strains, and displacements upon structural members or material samples. These loading conditions can be applied with DC to 70 Hz rates.

We integrated our sensor into a steel bar measuring 2.5 cm x 7.5 cm x 48 cm. Each end of the 48 cm length clamp into load frame grips. The test specimen is then loaded with sinusoidal tensile/compressive loads. We specify loading magnitude and frequency to deliver desired strain rates. For reference, we attach a strain gage within the VRT Strain Rate Sensor's gage length.

A photograph of the test setup at STL is in Figure 2. The STL load frame with strain rate sensor test piece can be seen at the right hand side of the figure. The figure also shows the Nicolet Digital Oscilloscope and the box containing all amplifiers, filters, and bridge circuits. We collected data on the 4 channel Nicolet scope. For all tests, we recorded three data records: measured strain rate, measured strain, and load frame applied force.

A closeup of the proof-of-principle strain rate sensor integrated with the test specimen is in Figure 3. A 4 cm x 6.35 cm window was machined in the middle of the bar. The strain rate sensor was attached on the

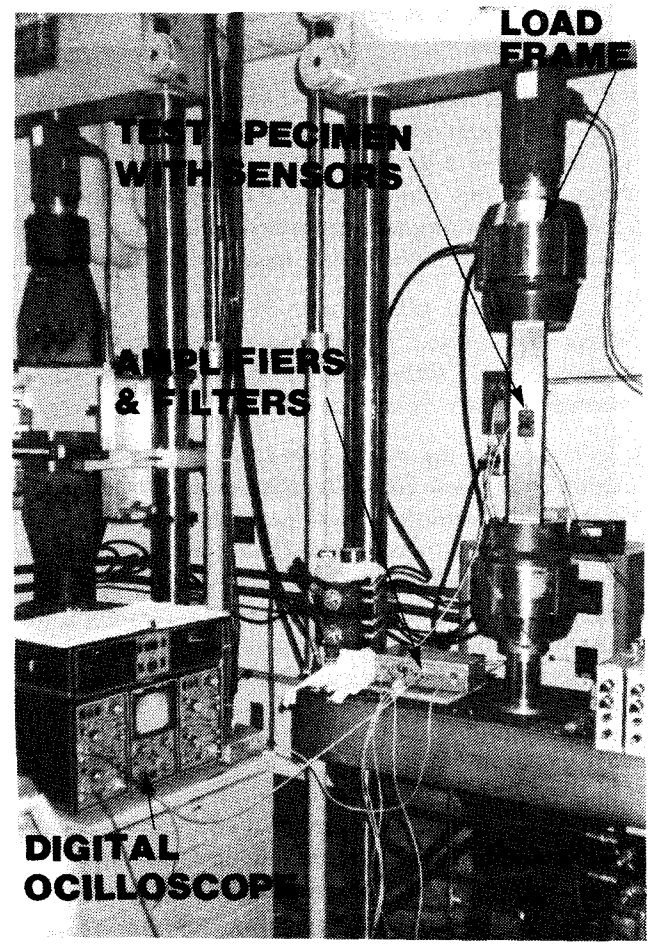

Fig. 2. Precision load frames were used to validate Strain Rate Sensor performance.

interior of this window. The ferrocores were fabricated from 1008 steel. The low carbon content implies high magnetic permeability. Stainless steel spacers magnetically isolate the ferrocores from the steel bar. Brass bolts attach the ferrocore halves to each end of the precision machined window in the steel test specimen. The sensor measures 2.5 cm x 3.5 cm x 5.1 cm (excluding stainless spacers). The sensor, as is in its non-optimal configuration, weighs about 125 grams.

The core faces each measure 0.95 cm so that the core area, A, is 0.90 cm^2. The output winding has 800 turns of 46 gage wire (51 μ diameter). The air gap length between core faces is 0.127 μm ($\pm$10%). The gage length or distance between attachment points is exactly 63.5 cm long. The ratio of gage length to gap length, K, is approximately 500. The magnetomotive force is supplied by 96 turns of excitation windings with 875 mA of constant current; the resulting nominal magnetic flux density, β_0, is about 0.5 Tesla (5000 gauss). With these parameters substituted into

Equation 14, the sensitivity of our experimental sensor (neglecting strain sensitivity) is given by,

$$\dot{\epsilon} \sim 50e^{-3} \cdot V_{out} \quad \epsilon/s \qquad (15)$$

Output from the sensor is amplified. We used two low noise, single op amp designs, one with a gain of 100, the other with a gain of 1000. Output noise in each design was less than 1 mV. After amplification, the strain rate sensor signal was filtered with a simple 200 Hz cutoff RC circuit. We directly measured the filtered data.

The strain gage is used in a single arm, 120 Ω Wheatstone bridge. The low noise bridge amplifier has a gain of 2500. Strain data was filtered at 1000 Hz and recorded directly by the Nicolet.

We use the strain gage data as a reference to qualitatively assess Strain Rate Sensor performance. We digitally differentiate strain gage data using a post-processing nearly equal ripple (NER) derivative filtering method[27]. The NER derivative filter was included in our commercially available post-processing data manipulation program. All differentiated strain data presented in the next section was derived with this approach.

Test Results

We chose data from two experiments to demonstrate bandwidth and resolution capabilities of our sensor. The first data set exemplifies high performance strain rate measurement capability. Strain rates are measured during 20 Hz, 16 μstrain oscillations in the beam. Twenty Hertz is as high as the load frames could oscillate while still maintaining good sinusoidal quality in the strain waveform. Peak strain rate magnitudes during this test were about $2e^{-3}$ ϵ/s. This magnitude is about 40 times greater than the resolution requirements discussed in the previous section. This strain rate typifies magnitudes during disturbance response in a structure.

Figure 4 shows an over-plot of strain gage and strain rate sensor output for the 20 Hz, 40 μstrain oscillation. Qualitatively, strain rate sensor output is as clean (if not cleaner) as strain gage output. Strain rate data is approximately 90^0 out-of-phase with strain data. The 200 Hz first order filter adds about six additional degrees of phase error to the 20 Hz strain rate data. This accounts for the minor phase discrepancies that are visible.

Figure 5 shows a comparison of digitally differentiated strain and strain rate sensor output from the same test. The strain rate signal is the single line; it is inverted for clarity. The differentiated strain data is exceedingly noisy. However, this graph is not intended as a comparison of differentiation versus direct measurement. This would only be fair if our differentiation algorithm was optimized for this application (the one we used surely was not). Filtering of the differentiated data could eliminate high frequency noise components; however, 60 Hz components still strongly distorted the filtered waveform. For this reason, we decided to simply show the unfiltered differentiated data. The two key points that we want to make with Figure 5 is that strain rate sensor output waveform appears accurate and is of high quality.

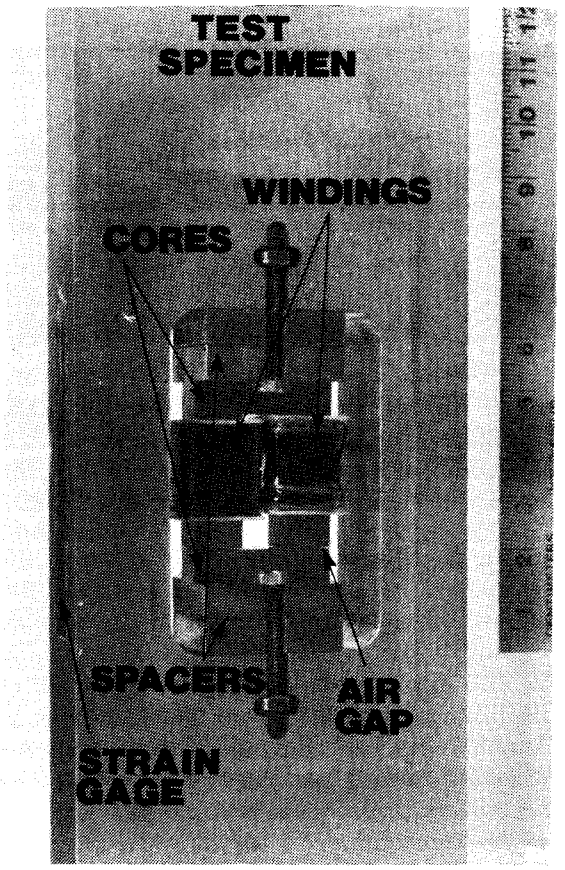

Fig. 3. The Strain Rate Sensor directly measures structural strain rates in the test specimens.

The second data set demonstrates resolution capability required for the applications discussed in the requirements section. This test measured strain rates occurring during 80 μstrain, 0.1 Hz beam oscillations. The corresponding strain rate magnitude is about 50 e^{-6} ϵ/s. The excitation frequency is much lower than our bandwidth objective. We chose 0.1 Hz since it is of the same magnitude of first boom bending modes on early space station configurations[28]. Very low frequency capability is essential.

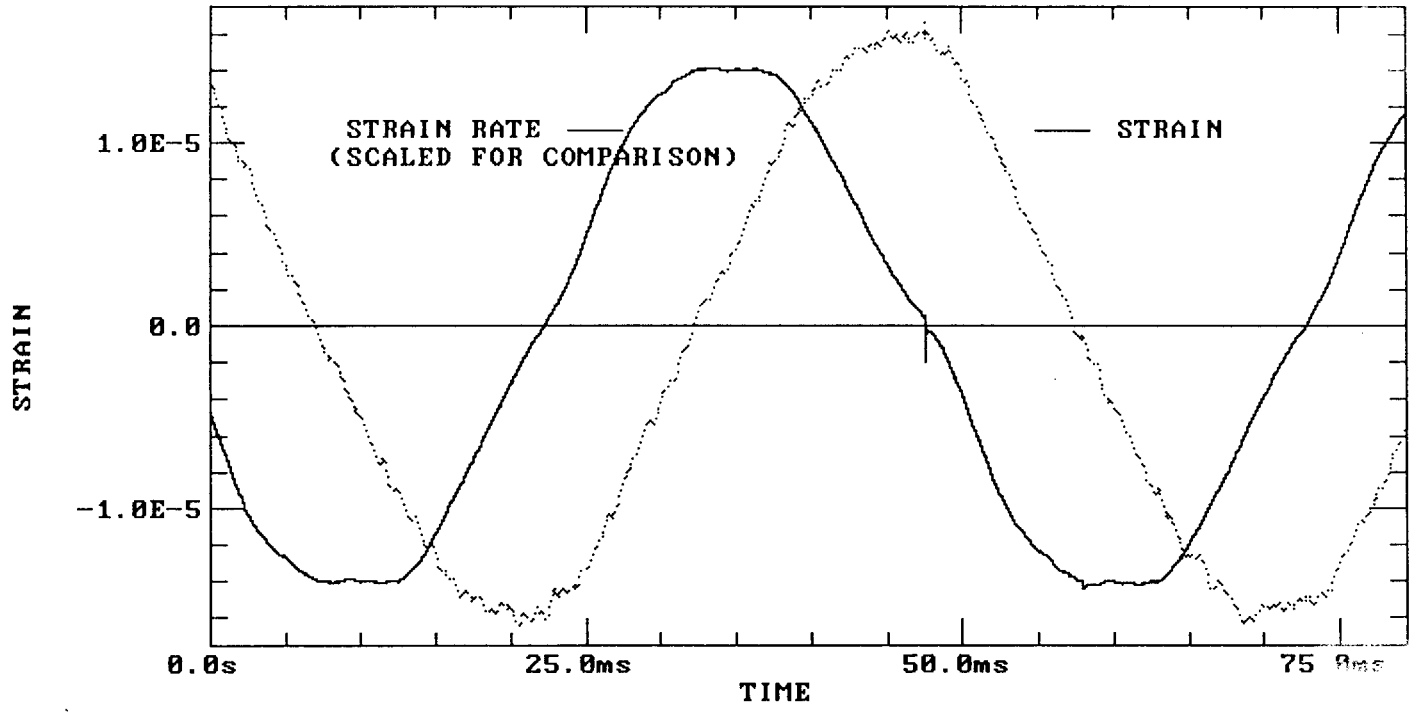

Fig. 4. Strain Rate Sensor output is very clean.

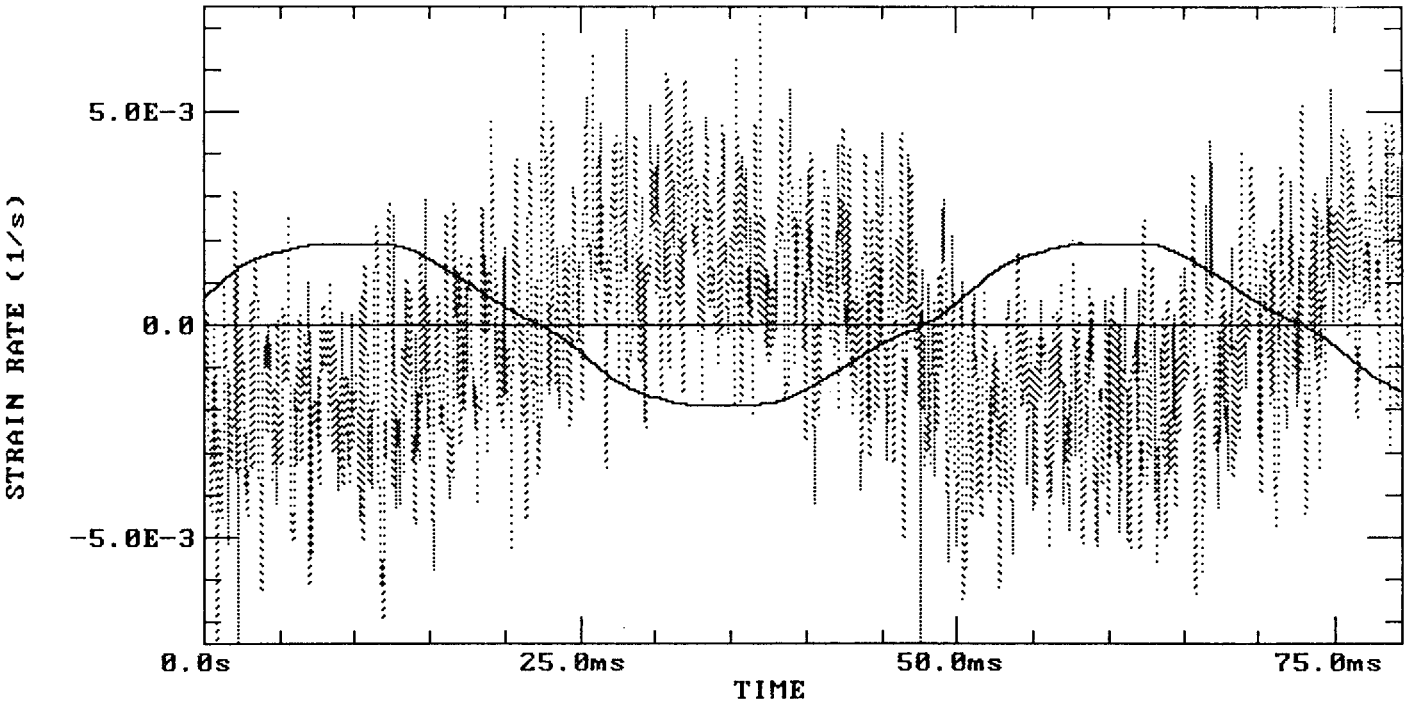

Fig. 5. Strain rate sensor output appears accurate and is of high quality (strain rate sensor output is the solid line, differentiated strain is the dotted line).

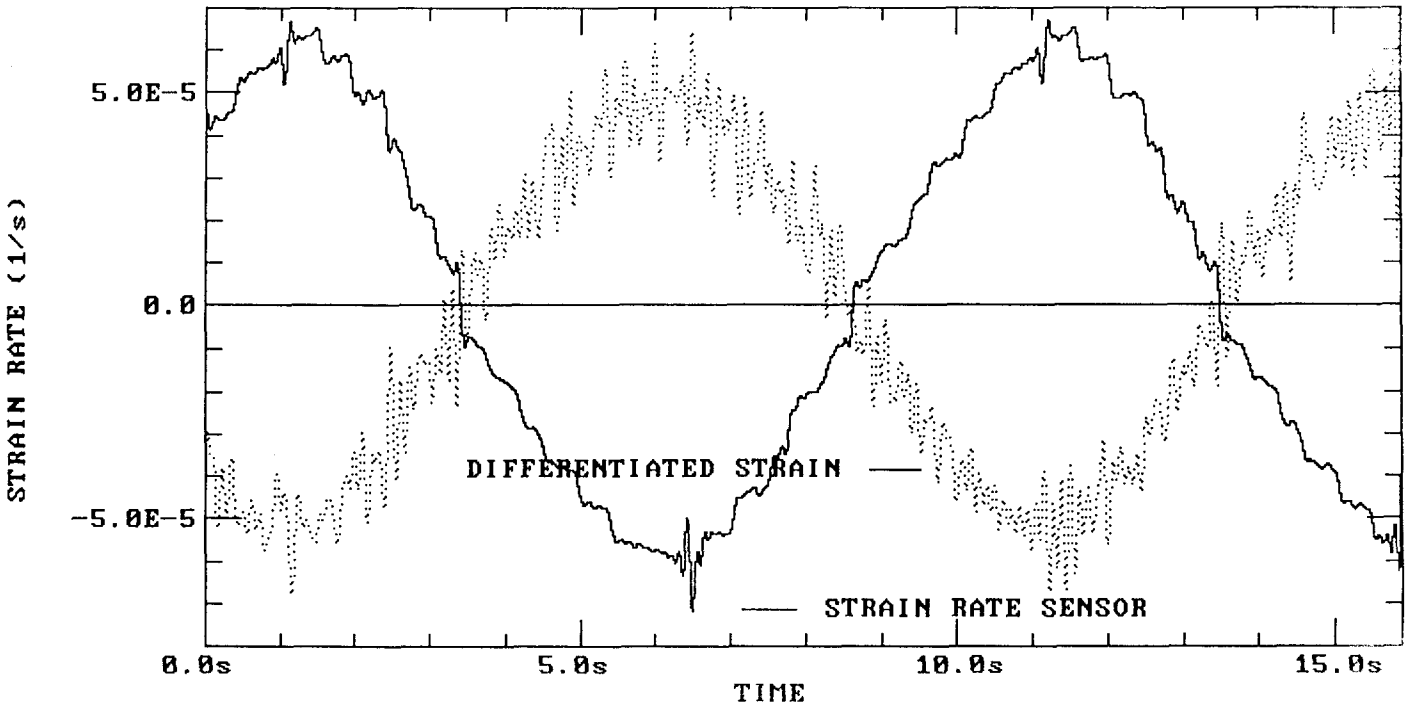

Fig. 6. **This strain rate sensor concept can measure very small strain rates and very low frequencies.**

A comparison of differentiated strain and direct strain rate sensor output for this test is in Figure 6. Both data signals in the figure were digitally filtered at 10 Hz. At this resolution, the unfiltered data from both signals was plagued by noise. The strain rate sensor signal appeared as noisy as the differentiated strain signal. The key difference was that strain rate sensor noise was made up entirely of 60 Hz content while differentiated strain noise was composed of wide bandwidth content. We later learned that a differential amplifier significantly reduced net noise in strain rate output. Nevertheless, the data in Figure 6 demonstrates high resolution and very low frequency measurement capabilities.

Sizing Estimates

The experiments demonstrate strain rate sensor bandwidth and magnitude capabilities. However, core and coil mass of 20 grams is excessive compared with our desirable 20 gram goal. In advanced sensor designs, the core and coil will be housed in an EM pickup shielding enclosure. These enclosures will probably be more massive than the core and coil themselves. In order for total package mass to come in under 20 grams, core and coil mass must be very small. The proof-of-principle sensor mass is far from optimal for its resolution capabilities. Mass efficient Strain Rate Sensors can meet S/N and resolution goals with very small core and coil mass. Here, we investigate resolution and sensor mass relationships for low mass sensor designs.

Low mass results from high winding density. Windings increase sensitivity; hence maximum sensitivity for a given geometry is achieved when most the windings possible are packed onto the ferrocore. From Figure 3, it is obvious that proof-of-principle designs do not have high density windings. In order to investigate low mass sensors, we define some simple geometric interrelationships.

Consider a generic strain rate sensor geometry in which the area of the window opening is the same as cross sectional area of ferrocores. The cross sectional area, A, of the ferrocores is square in this generic geometry. The proof-of-principle sensor core layout could easily resemble this geometry. Assume that the magnetomotive force is supplied by a permanent magnet and that no excitation windings are therefore required. Core windings might realistically occupy 55% of the window opening (this includes pack factor efficiency and a little left over room). Number of core turns is then expressed as

$$N = \frac{0.55\,A}{A_w} \tag{16}$$

where A_w = wire size.

Substituting into the sensitivity relation, Equation 14, gives

$$\frac{V_{out}}{\dot{\epsilon}} = \frac{-0.55\,K\,A^2\,\beta_0}{A_w} \tag{17}$$

From our experimental experience, we can chose realistic values for β_0, K, and A_w. A good value for magnetic flux density, β_0, is 0.5 Tesla. Ferromagnetic materials behave linearly in the 0 to 2 Tesla range. Our design value allows an ample margin for flux variations incurred during air gap motion.

In our experiments, the ratio of gage length to gap length, K, was about 500. Our gage length was quite large at 63.5 cm. Realistically, we anticipate much smaller gage lengths and correspondingly smaller gap lengths. Even if the sensor "footprint" is smaller than 1.3 cm we can use lightweight gage length extenders to obtain high K's. Here, we keep K at its experimental value of 500.

Microscopically small size "wire" may be used for the winding. However, transformer theory tells us bandwidth decreases as wire size decreases for a given core size[29]. We have not yet experienced any experimental bandwidth limitations; we conservatively chose 46 gage wire (51 μm diameter) for this feasibility inquiry.

The defined geometric relationships of our generic sensor uniquely define sensor mass as a function of core area. The copper windings wrap around a known cross sectional area, A, and have cross sectional area of their own that is 0.55 A. Core area, A, uniquely defines coil volume and hence, mass. Core mass is also uniquely defined by A. It can be shown that the sum of core and winding mass for this example geometry is given by

$$mass \sim 100\ A^{3/2} \tag{18}$$

where mass = grams, and
A = cm^2.

Substituting Equation 17 and the design values from the above paragraphs into Equation 18 and rearranging gives

$$mass \sim 3/4\ \left(\frac{V_{out}}{\dot{\epsilon}}\right)^{3/4} \tag{19}$$

Our interest is to examine mass predictions as a function of minimum sensor resolution and S/N ratio. Desirable output voltage at minimum resolution readings can be expressed as the product of noise voltages and S/N ratio,

$$V_{out} = (S/N)\ V_{noise} \tag{20}$$

where V_{noise} = sum of EM, thermal, and amplifier noise voltages.

Thermal noise for our application is insignificant compared with amplifier and EM pickup. The EM pickup mechanism is identical to our strain rate detection mechanism; changing flux in the coils produces a voltage across the coils. In our proof-of-principle experiments, EM pickup limited sensor resolution. However, we were not well shielded for these experiments. Performance after shielding is difficult to model. For this analysis, we assume that EM pickup is much less than amplifier noise. We have quantified data on amplifier performance from our proof-of-principle experiments. Our low-noise 1000 gain amplifier showed 1 mV of noise with shorted inputs. Reflecting amplifier noise to its input, a minimum resolution output voltage is defined as

$$V_{out} = 1e^{-6}\ (S/N) \tag{21}$$

Substituting into Equation 21 expresses sensor mass in terms of resolution and S/N,

$$mass \sim 25e^{-6}\ \left(\frac{S/N}{\dot{\epsilon}_{min}}\right)^{3/4} \tag{22}$$

Figure 7 shows a plot of this relation. For strain rate resolution to 25 e^{-6} e/s with 40 dB S/N, ferrocore and coil mass is only about 2.2 grams. If S/N is increased to 60 dB, core and coil mass increase to about 12.5 grams. These mass estimates do not include shielding mass; however, low core and coil mass leave adequate margin for shielding to meet a total sensor mass goal below 20 gram.

Summary of Testing and Sizing Results

Testing results indicate that our Strain Rate Sensor concept has resolution and bandwidth capabilities relevant to structural control applications. Furthermore, sizing estimates indicate that acceptable mass is achievable with desirable resolution and S/N capabilities. Taken together, these results demonstrate feasibility of IAP's low mass, high performance Strain Rate Sensor technology.

Unresolved Technical Issues

Resolving key technical issues is essential to our goal of low mass, high performance Strain Rate Sensor Prototype demonstrations. The three most significant technical issues are overcoming output nonlinearities, ensuring immunity to electromagnetic pickup, and developing attachment systems that guarantee accurate measurements. Linearity is one of our quality assurance parameters. Strain dependency in the denominator of our sensitivity equation clearly limits linearity. Its phase difference with strain rates distorts the strain rate sensor output waveform. We have ignored this effect in our proof-of-principle research; however, waveform distortions will be unacceptable in prototype designs. Since post processing is undesirable, we are seeking geometric alternatives to ensure waveform errors do not exceed our linearity goals.

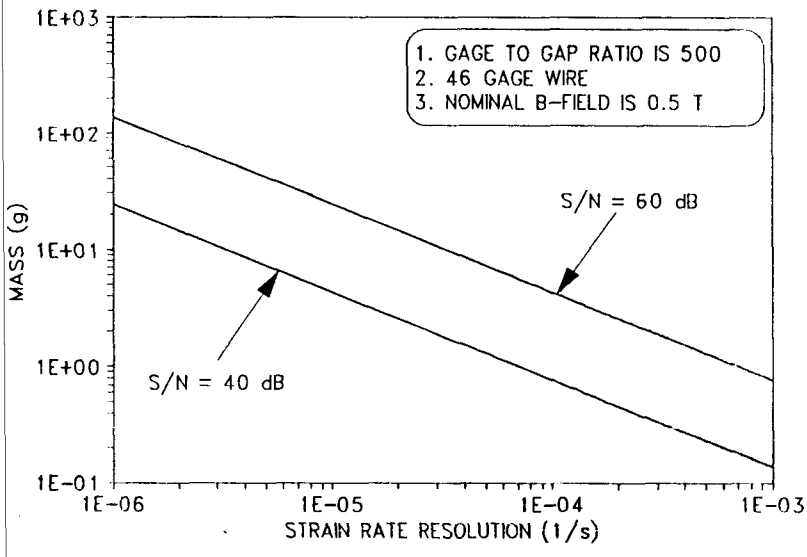

Fig. 7. Low sensor mass is achievable for structural control resolution requirements.

A coil of wire on a ferro-magnetic core makes a very good antenna. Pickup of external electromagnetic interference was a problem during strain rate sensor tests. It limited our usable sensor resolution during tests. As the sensor is made more sensitive to strain rates, it also becomes more sensitive to EM interference. High frequencies in the AM and FM regime can be filtered without ramifications. Low frequency pickup, particularly 60 Hz, is a much more severe problem. We are investigating shielding and geometric solutions to this problem.

Sensor attachment is also challenging. Preliminary finite element analysis indicated that epoxying the ferrocore halves to a flexible beam locally altered stress and strain contours. Clearly, this is undesirable. Smart strut applications are attractive in that we can better integrate sensor and structure. However, vibrating plate applications still seem to require a separate, attachable sensor.

Conclusions

In conclusion, IAP Research is developing a low mass, high performance Strain Rate Sensor to measure structural vibration rates. We have identified desirable performance characteristics for strain rate sensing on vibrating structures. Strain Rate Sensor proof-of-principle experiments have demonstrated bandwidth and magnitude capabilities relevant to the vibration control problem. Sizing estimates indicate that mass efficient designs will yield desirable Strain Rate Sensor mass. Continued successful development will result in an enabling sensor technology for vibration control of structures.

Acknowledgements

Our strain rate sensor research is funded by the Innovative Science and Technology Office of Strategic Defense Initiative Organization (SDIO) (Contract No. DACA88-90-C-0009). We also acknowledge the US Army Construction Engineering Research Laboratory (USA-CERL) in Champaign, IL for administering the contract. The authors also wish to acknowledge the contributions of IAP employees Rhoni Waggoner, Joseph Zeisler, and Neal Clements in preparation of this document.

References

1. Wada, Ben K. and Fanson, James L., "Adaptive Structures to Enable Future Missions by Relaxing Ground Test Requirements," 60th Shock and Vibration Symposium, Vol. 1, David Taylor Research Center, Portsmouth, VA, November 14-16, 1989.

2. Ramler, J. and Durrett, R., "NASA'S Geostationary Communications Platform Program," Proceedings of the AIAA 10th Communications Satellite Systems Conference, AIAA 84-0702, Orlando, FL, March 4, 1984.

3. AIAA Dynamics Specialist Conference, A Collection of Technical Papers, Long Beach, CA, April 5-6, 1990.

4. Hafta, Raphael T., "Integrated Structure-Control Optimization Of Space Structures," AIAA Dynamics Specialist Conference, Long Beach CA April 5-6, 1990.

5. Juang, Jer-Nan and Maghami, Peiman G., "Robust Eigensystem Assignments For Second-Order Dynamic Systems," AIAA Dynamics Specialist Conference, Long Beach CA April 5-6, 1990.

6. Junkins, John L. and Kim, Youdan, "A Minimum Sensitivity Design Method For Output Feedback Controllers," AIAA Dynamics Specialist Conference, Long Beach CA April 5-6, 1990.

7. Juang, J.N., Horta, L.G., and Robertshaw, H.H., "A Sewing Control Experiment for Flexible Structures," Proc. of the 5th VPI & SU Symposium on Dynamics and Control of Large Structures, pp. 547-551, Virginia Polytechnic Institute, Blackburg, VA, June 12-16, 1985.

8. Das, Alok, "Large Angle Maneuver Experiments In Ground-Based Laboratories," AIAA Dynamics Specialist Conference, Long Beach CA, April 5-6, 1990.

9. Sparks, Dean W., Jr., Horner, Garnett C., and Juang, Jer-Nan, "A Survey of Experiments and Experimental Facilities for Active Control of Flexible Structures," Third NASA/DoD CSI Technology Conference, San Diego CA, January 30 - February 2, 1989.

10. Junkins, J.L., Pollock, T.C., and Rahman, Z.H., "CSI Sensing and Control: Analytical and Experimental Results, Third NASA/DoD CSI Technology Conference, San Diego CA, January 30 - February 2, 1989.

11. Juang, J.N., Won, C.C., and Lee, C.K., "Shear Strain Rate Measurement Applied to Vibration Control of High-Rise Building," International Workshop on Intelligent Structures, Taipei, Taiwan, July 23-26, 1990.

12. Juston, John M., "Theoretical and Experimental Study into the Dynamics and Control of a Flexible Beam with a DC-Servo Motor Actuator, Master's Thesis " Virginia Polytechnic Institute and State University, Blackburg VA, October 1985.

13. Fanson, James, Blackwood, Gary, and Chu, Cheng-Chih, "Experimental Evaluation of Active-Member Control of Precision Structures," Third NASA/DoD CSI Technology Conference, San Diego CA, January 30 -February 2, 1989.

14. Ih, C-H, Wang, S., Bayard, D. and Eldred, D., "Adaptive-Control Experiments On A Large Flexible Structure," JPL NASA Tech Brief Vol. 14, No. 3, Item 159, March 1990.

15. Skidmore, G.R. and Hallauer, W.L., Jr., "Experimental-Theoretical Study of Active Damping With Dual Sensors and Actuators," Proceedings of the AIAA Guidance, Navigation, and Control Conference, AIAA, New York, 1985, pp. 433-442.

16. Joshi, S.M., "Robustness Properties of Colocated Controllers for Flexible Spacecraft," Journal of Guidance, Control, and Dynamics, Vo. 9, Jan.-Feb. 1986, pp. 85-91.

17. Balas, M., "Direct Output Feedback Control of LSS," J. Guidance Contr., Vol. 2, pp. 252-253, 1979.

18. Herceg, E.E., Handbook of Measurement and Control, Schaevitz Engineering, 1976.

19. Langer, B.F., "Design And Application of a Magnetic Strain Gage," Proc. Soc. Exper. Stress Analysis, Vol. 1, No. 2, 1943.

20. Strain Measuring System, U.S. Patent No. 2,361,173, Oct. 24, 1944.

21. Hetenyi, M., Handbook of Experimental Stress Analysis, John Wiley and Sons, Inc., New York, 1951.

22. Boggis, A. G., "Design Of Differential Transformer Displacement Gauges," Proc. of Soc. Expl. Stress Analysis, Vol. 9, No. 2, 1952.

23. Roberts, H.C., "Mechanical Measurements by Electrical Methods," The Instrument Publishing Co., Inc., Pittsburgh, 1951.

24. Fanson, J.L., Chu C-C., Smith, R.S., and Anderson, E.H., "Active Member Control of a Precision Structure with an H_∞ Performance Objective," AIAA-90-1224-CP Publication.

25. Personal communication with Dr. James Fanson, member Technical Staff, Applied Mechanics Technologies Section, Jet Propulsion Laboratory, Pasadena, CA.

26. Personal communication with Dr. H.H. Robertshaw, Professor of Mechanical Engineering, Virginia Tech, Blacksburg, VA.

27. Kaiser, J.F. and Reed, W.A., "Data Smoothing Using Low-Pass Digital Filters," Rev. Sci. Instrum., Vol. 48, No. 11, November 1977, pp. 1447-1457.

28. Ayers, J. Kirk, Cirillo, Daniel P., Giesy, Jay C., and et al., "Structural Dynamics and Attitude Control Study of Early Manned Capability Space Station Configurations," NASA Technical Memorandum 89078, January 1987.

29. Nordenberg, Harold M., "Electronic Transformer," Reinhold Publishing Corporation, New York, NY, 1964.